Density Functional Study of Protonated, Acetylated, and Mercurated Derivatives of Ferrocene: Mechanism of the Electrophilic Substitution Reaction

María J. Mayor-López and Jacques Weber*,†

Department of Physical Chemistry, University of Geneva, 30 quai Ernest-Ansermet, CH-1211 Geneva 4, Switzerland

Berit Mannfors

Department of Physics, P.O. Box 9, FIN-00014 University of Helsinki, Finland

Allan F. Cunningham, Jr.

Additives Division, Ciba Specialty Chemicals Research Marly SA, P.O. Box 64, CH-1723 Marly, Switzerland

Received March 24, 1998

The mechanism of the electrophilic substitution reaction of ferrocene has been investigated using density functional theory. In particular, reactions with two hard electrophiles (protonation and acetylation) and one soft electrophile (mercuration) have been studied at the LDA and B-PW91 levels of theory using a triple-ζ STO basis set. A general description of the reactions has been obtained, leading to results in agreement with experiment. Acetylation is found to occur via exo attack, whereas mercuration follows an endo mechanism. In the case of protonation, evidence for a rapid equilibrium between metal-protonated and agostic ring-protonated ferrocene is obtained, and no clear conclusion concerning the exo or endo mechanism can be deduced. The calculated proton affinities corresponding to both metal-protonated and agostic ring-protonated structures are in excellent agreement with experiment.

Introduction

The structure and reactivity of ferrocene have been a subject of numerous theoretical and experimental studies for many years. In particular, many computational studies has been reported for ferrocene and other metallocenes as well.[1−12] Second-order Moller−Plesset perturbation theory (MP2) and even configuration interaction (CI) calculations fail in reproducing the metal−ligand distance of ferrocene,[3,4] whereas a better agreement is obtained from Car−Parrinello, complete active space second-order perturbation theory (CASPT2) and coupled-cluster calculations.[2,10−12] The binding energy of ferrocene has also been calculated at different levels of theory, and agreement with experiment is good.[13,14] In ab initio studies, the use of large one-electron basis sets and the introduction of electron correlation increase dramatically the computational effort and, often, only partial optimization of geometry can be performed. In contrast, density functional theory (DFT) calculations allow a complete description of the various properties of ferrocene at a high level of theory.

As far as organometallic chemistry is concerned, ferrocene is an ideal prototype for metallocenes, due to the amount of experimental data reported so far for this molecule. Indeed, the crystal and molecular structures of ferrocene have been determined by X-ray diffraction[15] and gas-phase electron diffraction (ED);[16] vibrational Raman and infrared spectra have been recorded by several authors,[17] and electrophilic substitution reactions (protonation, acetylation, and mercuration) have been studied experimentally by Rosenblum et al.[18] and

† E-mail: Jacques.Weber@chiphy.unige.ch. Fax: ++ 41 (0) 22 702 65 18.

(1) Matsuzawa, N.; Seto, J.; Dixon, D. A. *J. Phys. Chem. A* **1997**, *101*, 9391.
(2) Koch, H.; Jørgensen, P.; Helgaker, T. *J. Chem. Phys.* **1996**, *104*, 9528.
(3) Lüthi, H. P. *J. Mol. Struct. (THEOCHEM)* **1996**, *388*, 299 and references therein.
(4) McKee, M. L. *J. Am. Chem. Soc.* **1993**, *115*, 2818.
(5) Berces, A.; Ziegler, T.; Fan, L. *J. Phys. Chem.* **1994**, *98*, 1584.
(6) Weber, J.; Flükiger, P.; Stussi, D.; Morgantini, P. Y. *J. Mol. Struct. (THEOCHEM)* **1991**, *227*, 175.
(7) Jungwirth, P.; Stussi, D.; Weber, J. *Chem. Phys. Lett.* **1992**, *190*, 29.
(8) Doman, T. N.; Hollis, T. K.; Bosnich, *J. Am. Chem. Soc.* **1995**, *117*, 1352.
(9) Doman, T. N.; Landis, C. R.; Bosnich, B. *J. Am. Chem. Soc.* **1992**, *114*, 7264.
(10) Margl, P.; Schwarz, K.; Blöchl, P. E. *J. Chem. Phys.* **1994**, *100*(11), 8194.
(11) Park, C.; Almlöf, J. *J. Chem. Phys.* **1991**, *95*, 1829.
(12) Pierloot, K.; Persson, B. J.; Roos, B. O. *J. Phys. Chem.* **1995**, *99*, 3465.
(13) Klopper, W.; Lüthi, H. P. *Chem. Phys. Lett.* **1996**, *262*, 546.
(14) Mayor-López, M. J.; Weber, J. *Chem. Phys. Lett.* **1997**, *281*, 226.
(15) Dunitz, J. D.; Orgel, L. E.; Rich, A. *Acta Crystallogr.* **1956**, *9*, 373.
(16) Haaland, A. *Acc. Chem. Res.* **1979**, *12*, 415.
(17) Bodenheimer, J. S.; Low, W. *Spectrochim. Acta* **1973**, *29A*, 1733 and references therein.
(18) Rosenblum, M.; Santer, J. O.; Howells, W. G. *J. Am. Chem. Soc.* **1963**, *85*, 1450.

10.1021/om980218i CCC: $15.00
Publication on Web 10/14/1998

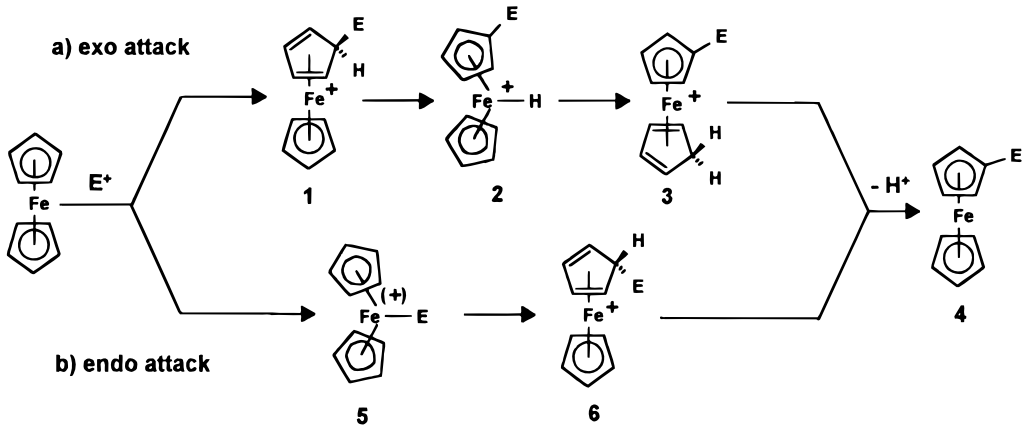

Figure 1. General mechanism of electrophilic substitution reactions of ferrocene.

Cunningham,[19−21] who conclude that hard electrophiles are likely to follow an exo reaction path whereas soft ones exhibit an endo attack (see Figure 1).

In view of the interest shown by experimentalists for the mechanism of electrophilic substitution reactions of ferrocene, it was tempting to also study them theoretically. Indeed, theoretical calculations represent an indispensable complement to experiment in view of a detailed description of such reaction mechanisms. Only one theoretical investigation has been performed so far on this type of reaction, namely the protonation of ferrocene.[4] Due to the recent success of DFT methods in producing reliable results for the structural and energetic properties of organometallics,[22] it is challenging to apply this model to ferrocene. Therefore, we have investigated in this paper the electrophilic substitution reactions of ferrocene ($FeCp_2$) with hard (proton H^+ and acetyl cation CH_3CO^+) and soft (mercury cation Hg^{2+}) electrophiles using DFT. To find out the most probable mechanism (exo or endo) for protonation, acetylation, and mercuration, the corresponding critical points on the potential energy surfaces have been identified. For the protonated species vibrational frequencies have been calculated to characterize the optimized stationary points.

Computational Details

All calculations were performed using the Amsterdam density functional (ADF) package developed by Baerends et al.[23−25] The numerical integration procedure was that of te Velde et al.[25,26]

An uncontracted triple-ζ STO basis set[27] was used for the 3d and 4s orbitals of the iron atom, for the 5d and 6s orbitals of the mercury atom, for the 2s and 2p orbitals of the carbon and oxygen atoms, and for the 1s orbital of the hydrogen atoms. For the 3s and 3p orbitals of the iron atom, a double-ζ STO basis set was used. This basis set was augmented by a p function in the case of Fe and Hg atoms, whereas for C and O atoms an extra d polarization function and for H atoms an extra p function were added (basis set IV in the ADF code). The inner cores of iron (1s2s2p), mercury (1s2s2p3s3p3d4s-4p4d4f5s5p), carbon (1s), and oxygen (1s) were treated with the frozen-core approximation.[24] A set of auxiliary s, p, d, f, and g STO functions,[28] centered on all nuclei, was used to fit the molecular density and represent the Coulomb and exchange potentials accurately in each SCF cycle. The quasi-relativistic approach, as implemented in the ADF code,[29,30] was used to take into account relativistic effects in the calculations of mercurated species.

Geometry optimizations were first carried out at the LDA (local density approximation)[31] level with the VWN (Vosko−Wilk−Nusair)[32] approximation. The most stable structures obtained at the LDA level (as well as some other particular cases) were then reoptimized at a higher level of theory by including gradient-based corrections to the exchange and correlation potentials due to Becke[33] and Perdew and Wang[34] (B-PW91), respectively, in the SCF procedure.[35] Force constants and vibrational frequencies were calculated at the corresponding levels of theory to characterize the stationary points. The convergence criteria applied during the geometry optimizations were 10^{-4} hartrees for the energy and 10^{-3} hartree/Å for the gradients. Only nonhybrid functionals are available in the ADF package.

Since ADF molecular energies actually represent bonding energies between fragments,[36] the same fragments must be used as building blocks for the various structures of the systems in order to have meaningful results.

Results and Discussion

To find out the most adequate level of theory able to describe properly the electrophilic substitution reaction mechanism, the structure of ferrocene was studied first.

1. Ferrocene. Two conformations with respect to the relative orientation of the cyclopentadienyl (Cp) ligands, eclipsed (D_{5h}) and staggered (D_{5d}), are conceivable for ferrocene. Their geometries were completely

(19) Cunningham, A. F., Jr. *J. Am. Chem. Soc.* **1991**, *113*, 4864.
(20) Cunningham, A. F., Jr. *Organometallics* **1994**, *13*, 2480.
(21) Cunningham, A. F., Jr. *Organometallics* **1997**, *16*, 1114.
(22) Ziegler, T. *Can. J. Chem.* **1995**, *73*, 743.
(23) ADF 2.0.1; Department of Theoretical Chemistry, Vrije Universiteit, Amsterdam, The Netherlands, 1995.
(24) Baerends, E. J.; Ellis, D. E.; Ros, P. *Chem. Phys.* **1973**, *2*, 41.
(25) te Velde, G.; Baerends, E. J. *J. Comput. Phys.* **1992**, *99*, 84.
(26) Boerritger, P. M.; te Velde, G.; Baerends, E. J. *Int. J. Quantum Chem.* **1988**, *33*, 87.
(27) Vernooijs, P.; Snijders, G. J.; Baerends, E. J. *Slater Type Basis Functions for the Whole Periodic System*; Internal Report, Freie Universiteit Amsterdam, Amsterdam, The Netherlands, 1981.
(28) Krijn, K.; Baerends, E. J. *Fit Functions in the HFS Method*; Internal Report, Freie Universiteit Amsterdam, Amsterdam, The Netherlands, 1984.
(29) Boerritger, P. M. Spectroscopy and Bonding of Heavy Element Compounds. Ph.D. Thesis, Chemistry, Vrije Universiteit, Amsterdam, The Netherlands, 1987.
(30) Ziegler, T.; Tschinke, V.; Baerends, E. J.; Snijders, J. G.; Ravenek, W. *J. Phys. Chem.* **1989**, *93*, 3050.
(31) Gunnarsson, O.; Lundquist, I. *Phys. Rev.* **1974**, *B10*, 1319.
(32) Vosko, S. H.; Wilk, L.; Nusair, M. *Can. J. Phys.* **1980**, *58*, 1200.
(33) Becke, A. D. *Phys. Rev.* **1988**, *A38*, 3098.
(34) Perdew, J. P. In *Electronic Structure of Solids '91*; Ziesche, P., Eschrig, H., Eds.; Academie Verlag: Berlin, 1991; p 11.
(35) Fan, L.; Ziegler, T. *J. Chem. Phys.* **1991**, *94*, 6057.
(36) Ziegler, T.; Rauk, A. *Theor. Chim. Acta* **1977**, *49*, 143.

Table 1. Structural Features of Eclipsed (D_{5h}) and Staggered (D_{5d}) Conformations of Ferrocene at the LDA and B-PW91 Levels of Theory

		eclipsed Cp's		staggered Cp's	
	exptl[a]	LDA	B-PW91	LDA	B-PW91
		Distances d (Å)			
Fe−X[b]	1.660	1.606	1.661	1.612	1.666
Fe−C	2.064	2.012	2.061	2.016	2.065
C−C	1.440	1.425	1.435	1.424	1.434
C−H	1.104	1.091	1.086	1.091	1.086
		Angles α (deg)			
X−Fe−X′ [b]		180.0	180.0	180.0	180.0
H−X−C[c]	−3.7	−0.6	−0.3	−0.7	−0.5
		Angles θ (deg)			
H−C−C′−H′ [b]		0.0	0.0	35.8	35.6
		Energy[d]			
		−5.300 968	−4.866 925	−5.298 800	−4.865 316
		−3326.41	−3054.04	−3325.05	−3053.03

[a] Reference 16. [b] X and X′ are dummy atoms located in the center of each Cp ring. Similarly, C−H and C′−H′ refer to bonds belonging to different Cp rings. [c] A positive value of this angle means that the H atoms are out of the plane of the Cp ligands away from the Fe atom. [d] Energy relative to the spherically averaged ground-state atomic fragments. The first entry is given in au and the second in kcal/mol.

optimized at both the LDA and B-PW91 levels of theory (Table 1). The stationary points were characterized by vibrational analysis. It is known from experiment that $FeCp_2$ adopts an eclipsed conformation in the gas phase,[16] whereas staggered Cp rings are observed in single crystals.[15] A very low energy barrier (0.9 ± 0.3 kcal/mol) for the internal rotation of the Cp ligands[37] is also predicted by gas-phase ED. From our calculations and in agreement with ED results, the eclipsed conformation is the global minimum on the potential energy surface of the internal rotation of ferrocene, whereas the staggered conformation with one imaginary frequency (31i cm^{-1}) corresponding to the normal mode of internal rotation is a transition state. The energy difference between staggered and eclipsed conformations is 1.0 (1.4) kcal/mol at the B-PW91 (LDA) level, which together with the low value of the imaginary frequency stands for the shallowness of the potential energy surface and agrees well with the low barrier for internal rotation predicted by the ED experiment.

The calculated values of the geometrical parameters are also in good agreement with experiment.[16] As expected, LDA leads to shorter bond lengths due to the well-known overbinding effect, but the results are still in good agreement with experiment. This is corrected by the B-PW91 functional, and in fact, the metal−ligand distance in the eclipsed conformation is then only 0.001 Å longer than the experimental value. However, the calculated bending angle of the H atoms toward Fe is too small but is in the right direction (0.6 and 0.3° at the LDA and B-PW91 levels, respectively, whereas the experimental values are 3.7(9) and 1.6(4)° by electron and neutron diffraction,[16,38] respectively). Recently, Matsuzawa et al.[1] have also optimized the eclipsed and staggered structures of ferrocene using DFT. Their results at the local level are in agreement with our LDA results, whereas significant differences in the metal−ligand distance are found in results with nonlocal corrections. The metal−ligand distance for the eclipsed conformation obtained by Matsuzawa et al. is calculated 0.043 Å too long (1.703 Å), whereas ours is only 0.001 Å longer than the experimental ED value. The energy differences between the staggered and eclipsed conformations by Matsuzawa et al. (1.1 and 0.5 kcal/mol at the local and nonlocal levels, respectively) are calculated to be 0.3 and 0.5 kcal/mol lower than our values. As a conclusion, the results presented in Table 1 suggest that the level of theory used in our calculations allows an accurate description of the structure and energetics, which is a prerequisite for the calculation of the mechanism of the electrophilic substitution reaction.

2. Electrophilic Substitution of Ferrocene. As reported in the experimental studies of Cunningham,[19−21] one expects hard electrophiles to attack ferrocene on the exo face of one Cp ring (exo attack), whereas soft electrophiles should first precomplex the metal atom and then attack the Cp ring on its endo face (endo attack). Figure 1 shows the probable mechanism of both these attacks. In this paper, DFT methodology is used to elucidate the mechanisms of protonation, acetylation, and mercuration of ferrocene and in particular to identify short-lived intermediates that cannot be trapped by experimental techniques.

2.1. Protonation of Ferrocene. Protonation of ferrocene is an electrophilic substitution reaction by a hard electrophile, and it should therefore occur via exo attack. The NMR experiments in boron trifluoride hydrate reported by Curphey et al.[39] have shown that only a metal-protonated form is observed in solution. Experiments performed with a mixture of heavy water and nitrogen gas also conclude to metal attack of the deuterium cation without exchange with the Cp hydrogens.[40] However, the existence of two protonated forms was also suggested. In this case, the metal-protonated form should be by at least 5 kcal/mol more stable than the ring-protonated one.[40] In contrast, experiments in deuterated media showed a rapid equilibrium between ring- and metal-protonated forms in ferrocene.[41] Thus, preference for exo or endo attack cannot be elucidated by these experiments.

(37) Haaland, A.; Nilsson, J. E. *Acta Chem. Scand.* **1968**, *22*, 2653.
(38) Takusagawa, F.; Koetzle, T. F. *Acta Crystallogr., Sect. B* **1979**, *35*, 1074.
(39) Curphey, T. J.; Santer, J. O.; Rosenblum, M.; Richards, J. H. *J. Am. Chem. Soc.* **1960**, *82*, 5249.
(40) Meot-Ner, M. *J. Am. Chem. Soc.* **1989**, *111*, 2830.

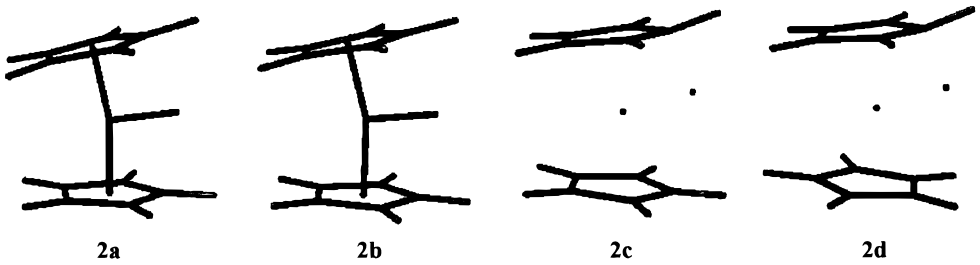

Figure 2. LDA (**2a**) and B-PW91 (**2b**) structures for eclipsed metal-protonated ferrocene and B-PW91 structures for the eclipsed (**2c**) and staggered (**2d**) conformers of (agostic) ring-protonated ferrocene.

Table 2. Structural Features of the Most Stable Conformation (Eclipsed Cp's/Eclipsed H^+) of Metal-Protonated Ferrocene $[FeHCp_2]^+$ at the LDA and B-PW91 Levels of Theory (2a and 2b) and the Eclipsed and Staggered Conformers of (Agostic) Ring-Protonated Ferrocene $[FeCp_2H]^+$ at the B-PW91 Level of Theory (2c and 2d)

	2a (LDA)	**2b** (B-PW91)	**2c** (B-PW91)	**2d** (B-PW91)
		Distance *d* (Å)		
Fe−X[a]	1.637	1.695	1.683/1.693[b]	1.686/1.698
Fe−H^+	1.488	1.495	1.561	1.586
Fe−C	2.032−2.041	2.080−2.093	2.039−2.102	2.037−2.111
C−C	1.414−1.431	1.424−1.442	1.416−1.468	1.414−1.473
C−H	1.090−1.093	1.085−1.087	1.086−1.091	1.086−1.093
C−H^+	1.822	1.879	1.422	1.358
		Angles α (deg)		
X−Fe−X′ [a]	167.2	166.9	168.5	167.9
X−Fe−H^+	96.4	96.6	81.4	79.3
		Angles *θ* (deg)		
H−C−C′−H′ [a]	0.0	0.0	0.0	27.8
H−C−Fe−H^+	0.0	0.0	0.0	0.1
		Energy[c]		
	−5.189 418	−4.748 728	−4.748 307	−4.746 998
	−3256.41	−2979.87	−2979.61	−2978.79

[a] X and X′ are dummy atoms located in the center of each Cp ring. Similarly, C−H and C′−H′ refer to bonds belonging to different Cp rings. [b] The first value is the metal to upper or substituted ring distance; the second value is that corresponding to the lower or unsubstituted one. [c] Energy relative to the spherically averaged ground-state atomic fragments. The first entry is given in au and the second in kcal/mol.

(i) Metal-Protonated Ferrocene. Four stable conformers may result from the metal protonation of ferrocene, depending on the eclipsed or staggered conformation of the Cp rings and the relative eclipsed or staggered position of the proton with respect to one C atom. All the geometries were completely optimized at the LDA level of theory. The most stable one exhibits C_{2v} symmetry with eclipsed Cp rings and an eclipsed H^+ (Figure 2), and it was further optimized at the B-PW91 level. The LDA and B-PW91 geometrical parameters for this structure are summarized in Table 2 and the structures shown in Figure 2 (structures **2a**,**b**). Characterization as minima on the potential energy surfaces was evidenced by vibrational analysis. The molecule is bent (167.2° at the LDA level and 166.9° at the B-PW91 level) as compared to the neutral ferrocene so as to reduce steric hindrance due to the incoming proton. The metal−ligand distances are about 0.03 Å longer than in $FeCp_2$ in order to minimize the Cp−Cp steric hindrance resulting from the Cp−Fe−Cp bending. The C−C bond lengths vary between 1.414 and 1.431 Å at the LDA level and between 1.424 and 1.442 Å at the B-PW91 level, indicating a slight decrease of the aromaticity of the invidual Cp rings.

(ii) Ring-Protonated Ferrocene. Two conformers, eclipsed and staggered with respect to the relative position of the Cp rings, are possible for ring-protonated ferrocene. As opposed to the previous case, the results obtained for the ring-protonated species are more sensitive to the level of theory. Actually, none of the geometry optimizations leads to a pure ring-protonated form. At both the LDA and B-PW91 levels the calculations exhibit an agostic structure in which the proton is located between the ring and the metal when the geometry of the conformer with staggered Cp rings is optimized (structure **2d**). In the case of the eclipsed conformer, the optimization at the LDA level leads to a metal-protonated structure identical with that obtained in the previous section (structure **2a**), whereas another agostic form emerges from the B-PW91 calculations (structure **2c**). The results are summarized in Table 2 and the structures shown in Figure 2.

All the agostic structures were characterized by vibrational analysis. For the LDA agostic form with staggered Cp rings an imaginary frequency (78i cm^{-1}) corresponding to the normal mode of internal ring rotation is obtained. At the B-PW91 level, the structure with staggered Cp's, **2d**, also presents a low imaginary frequency (26i cm^{-1}) corresponding to the same vibration. The eclipsed form **2c** at the B-PW91 level, instead, has only positive eigenvalues. It is therefore another minimum on the B-PW91 potential energy surface of protonation of $FeCp_2$, the other one being the (eclipsed) metal-protonated form **2b**. The energy difference be-

(41) Müller-Westerhoff, U. T.; Haas, T. J.; Swiegers, G. F.; Leipert, T. K. *J. Organomet. Chem.* **1994**, *472*, 229.

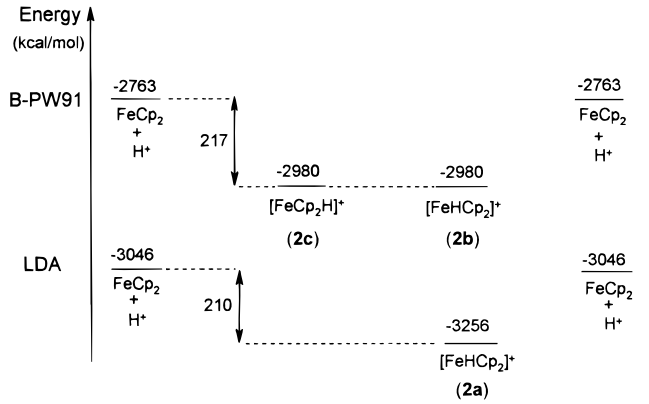

Figure 3. Critical points on the potential energy surface of protonated ferrocene.

tween staggered and eclipsed conformations of the ring-protonated (agostic) B-PW91 structures (**2d** and **2c**, respectively) is 0.8 kcal/mol (without zero-point energy (ZPE) corrections), which together with the low imaginary frequency obtained for the staggered conformation underlines the shallowness of the potential energy surface with respect to the internal rotation of the Cp ligands. The energy difference between the B-PW91 minima **2b** and **2c** is only 0.3 kcal/mol without ZPE corrections. A transition state, lying at practically the same energy as the two minima, is also found with a large negative eigenvalue of the Hessian matrix leading to an imaginary frequency of 236i cm^{-1} that corresponds to the motion of the proton between the agostic and metal-protonated orientations. The most relevant geometrical parameters of this structure are the inequivalent X−Fe−H^+ and X′−Fe−H^+ angles (96.1 and 97.8°, respectively), which arise from the breaking of C_{2v} symmetry on going from **2b** toward **2c** (X and X′ are dummy atoms located in the center of each Cp ring). Otherwise, the structural features are practically the same as those of **2b**. Including ZPE corrections, the energies of both minima (**2b** and **2c**) became equal, however, within the limits of accuracy of our calculations, indicating an extremely shallow energy profile. The DFT calculations do not, thus, really elucidate if the mechanism of the protonation reaction is exo or endo, as the metal-protonated structure can be either the result of precomplexation of the electrophile with the metal in the first step of an endo mechanism (**5** in Figure 1) or the one originating from the transfer of one of the H atoms from the exo-attacked ring toward the metal atom (**2** in Figure 1). The similar energies of the metal-protonated and agostic ring-protonated structures, as well as the low-lying transition state, indicate a rapid transfer of the proton between the metal and the Cp ring, as found also experimentally by H/D exchange.[41] Figure 3 shows the critical points on the potential energy surface of protonated ferrocene.

Concerning the geometries of the eclipsed structures at the B-PW91 level, the metal to protonated ligand distance in **2c** increases by 0.022 Å with respect to $FeCp_2$ due to the presence of an additional H between Fe and the upper ring. The bending angle is 168.5°, as compared to the linear $FeCp_2$ molecule. The Cp rings keep their planarity in both the **2b** and **2c** protonated cases, and only the H atom next to the agostic proton in **2c** is slightly bent outward from it. The aromaticity of the individual Cp rings is lost by ring protonation of ferrocene. In general, the structures of both **2b** and **2c** are close to each other due to the similar locations of the proton in both cases.

According to the ab initio calculations of McKee,[4] the metal-protonated form is preferred to the ring-protonated one by 34.6 kcal/mol at the MP2 level, whereas the situation is reversed at the HF level, the energy differences varying from 10 to 60 kcal/mol depending on the level of calculation. Concerning the geometries, the metal-protonated $FeCp_2$ is linear at the HF level, whereas it is bent at the MP2 level (bending angle 153.1°). Our B-PW91 structure for the metal-protonated $FeCp_2$ is intermediate between the HF and MP2 geometries of McKee. According to our results, the Cp ligands keep a more aromatic character than in the calculations of McKee. With regard to the ring-protonated conformer obtained at the HF level by McKee, the substituted ring remains unchanged with respect to the unsubstituted one. The MP2 calculations give, instead, a very distorted structure for the substituted ring.

(iii) Proton Affinity of Ferrocene. The gas-phase proton affinity (PA) of a molecule B is defined as the negative of the change of enthalpy at room temperature for the reaction

$$B + H^+ \rightarrow BH^+ \qquad PA \equiv -\Delta H_{298} \tag{1}$$

In the case of metal-protonation the reaction used to calculate PA of ferrocene is

$$FeCp_2\ (D_{5h}) + H^+ \rightarrow [FeHCp_2]^+\ (C_{2v}) \tag{2}$$

ZPE corrections have to be taken into account in the calculations of PA, and for the metal-protonated case the change in enthalpy can be written as

$$\Delta H_{298}(2) = \{E([FeHCp_2]^+) + ZPE([FeHCp_2]^+)\} - \{E(FeCp_2) + ZPE(FeCp_2) + E(H^+)\} \tag{3}$$

The calculations were performed at the LDA and B-PW91 levels of theory on the optimized structures presented in the previous sections. Thus, in the case of ring-protonated ferrocene only the B-PW91 results are given. The energies E in the equation above are bonding energies relative to the spherically averaged ground-state atomic fragments. The results are presented in Table 3. The thermal corrections are small, 1 kcal/mol in each case. The PAs obtained at the B-PW91 level for both the metal- and (agostic) ring-protonated structures are very close to each other. This is due to the almost equal energies of these structures (ΔE = 0.3 kcal/mol, and 0.0 kcal/mol with ZPE corrections). The calculated PA's show a good agreement with experiment.[40] However, they are at variance with the results of McKee,[4] which lead to the surprisingly overestimated result of 250.9 kcal/mol for the most stable metal-protonated form (MP2 results).

2.2. Acetylation of Ferrocene. Due to the hard character of the incoming electrophile, acetylation of ferrocene is expected to be an exo electrophilic substitution reaction and the experimental results[19,20] suggest

Table 3. Proton Affinities of Metal-Protonated and (Agostic) Ring-Protonated Ferrocene

	metal protonated (**2a**, **2b**)		agostic (**2c**)	
value, kcal/mol	LDA[a]	B-PW91[a]	B-PW91[a]	exptl[b]
$E([FeHCp_2]^+)$	−3256	−2980	−2980	
$ZPE([FeHCp_2]^+)$	+109	+109	+108	
$E(FeCp_2)$	−3326	−3054	−3054	
$ZPE(FeCp_2)$	+103	+103	+103	
$E(H^+)$	+280	+291	+291	
$\Delta H_{298}(2)$	−204	−211	−212	
proton affinity (PA)	204 (−3)[c]	211 (+4)[c]	212 (+5)[c]	207 ± 1
$\Delta E_{thermal}$[d]	−1	−1	−1	
$\Delta H_{298}(2) + \Delta E_{thermal}$	−205	−212	−213	
proton affinity (PA)[e]	205 (−2)[c]	212 (+5)[c]	213 (+6)[c]	207 ± 1

[a] Level of theory used in the geometry optimization and in the energy calculations. [b] Reference 40. [c] The values in parentheses correspond to the differences between calculated and experimental values. [d] $\Delta E_{thermal}$ is the thermal correction to the enthalpy of reaction 2. [e] Including thermal corrections to the enthalpy.

Table 4. Structural Features of the Acetylated Species at the LDA Level of Theory

	4a	**4b**	**4c**	**4d**	**4e**	**4f**
			Distances *d* (Å)			
Fe−X[a]	1.778/1.702[b]	1.671/1.670	1.610/1.637	1.603/1.639	1.624/1.631	1.602/1.611
Fe−H$^+$					1.668	
C−C	1.399−1.503	1.413−1.428	1.406−1.499	1.407−1.498	1.412−1.440	1.419−1.436
C−H	1.083−1.104	1.090−1.092	1.090−1.103	1.090−1.110	1.090−1.095	1.090−1.092
$C-C_{acetyl}$			1.658	1.645	1.481	1.460
$Fe-C_{acetyl}$	1.883	2.122				
			Angles α (deg)			
X−Fe−X′ [a]	153.1	157.2	174.7	174.5	168.7	179.2
$X-Fe-C_{acetyl}$	86.6	101.4				
X−Fe−H$^+$					104.5	
			Energy[c]			
	−6.431 409	−6.440 643	−6.427 385	−6.427 976	−6.453 107	−6.568 717
	−4035.77	−4041.56	−4033.25	−4033.62	−4049.39	−4121.93

[a] X and X′ are dummy atoms located in the center of each Cp ring. [b] The first value is the metal to the upper or substituted ring distance; the second value is that corresponding to the lower or unsubstituted one. [c] Energy relative to the spherically averaged ground-state atomic fragments. The first value is given in au and the second in kcal/mol.

that the reaction mechanism corresponds to the pathway (a) of Figure 1.

All the structures were first calculated at the LDA level. Then the stable conformations obtained along the reaction path were optimized at the B-PW91 level. On the basis of the results obtained for protonation, the eclipsed conformation of the ligands was taken as a starting point for our calculations. Due to the low barrier of the methyl rotation in acetyl chloride, the methyl group was constrained to its cis conformation (position of one of the H atoms of the methyl group relative to the C═O bond) when looking for stationary points in geometry optimizations (on the basis of the LDA and B-PW91 results for acetyl chloride in which the cis conformation was found to be more stable than the trans conformation by 1.0 and 0.9 kcal/mol, respectively, due to conjugation).

Both exo and endo approaches were considered at the LDA level. The results obtained at the LDA level are given in Table 4 and the structures shown in Figure 4. The two stable metal-acetylated structures **4a** and **4b** were obtained for the first step of the endo mechanism (**5** in Figure 1). **4b** is more stable than **4a** by 5.8 kcal/mol. Concerning the first step of the exo attack (**1** in Figure 1), the two stable structures **4c** and **4d** of practically equal energies were obtained. In both of them the acetyl backbone is perpendicular to the cycle, but they differ in the location of the O atom relative to the ring. The metal to substituted ring distances are shorter than those between the metal and the unsubstituted ring, which may be rationalized by a larger metal to ligand electron donation for the substituted ring due to the electron-withdrawing acetyl group. These two structures are about 8 kcal/mol higher in energy than the most stable metal-acetylated form **4b**.

With regard to the second steps of these reaction mechanisms (**2** and **6** in Figure 1), no stable structure was found for the endo mechanism (**6** in Figure 1), implying that $C_{ring}-C_{acetyl}$ bond formation and loss of H^+ occur simultaneously. The situation is different for the exo case. When the proton moves toward the metal atom (**2** in Figure 1), the stable intermediate **4e** was found. There is no experimental evidence for this intermediate. The acetyl backbone is now orthogonal to the ring, and the oxygen atom points toward the proton bonded to the metal atom, leading to a five-membered ring $Fe-H-O=C_{acetyl}-C_{ring}$. The coordination of the acetylated ligand to the metal does not modify the preferred cis conformation of the electrophile. As **4e** is a metal-protonated ferrocene with a substituted Cp ring, comparison with the **2a** structure is possible. The metal−proton bond length in **4e** is 0.180 Å longer than in **2a**, due to the electrostatic interaction with oxygen and to the lower electron density in the Fe−H$^+$ bond in **4e**. The bending angle is 1.5° larger and the metal−ligand distances are 0.013 and 0.006 Å shorter for the substituted and unsubstituted ligands, respectively, as compared with those for **2a**. Substitution

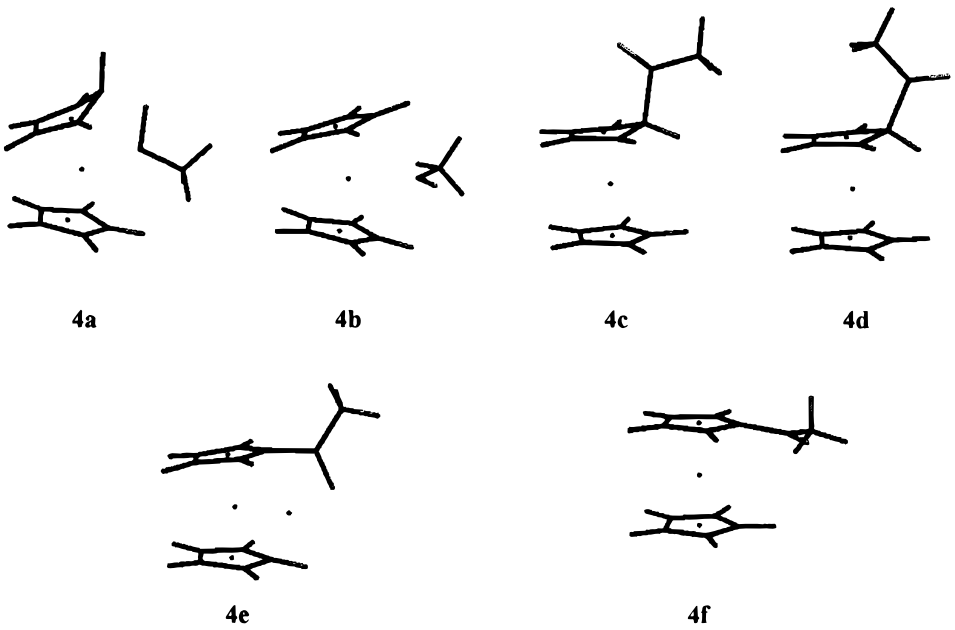

Figure 4. LDA structures for acetylated species.

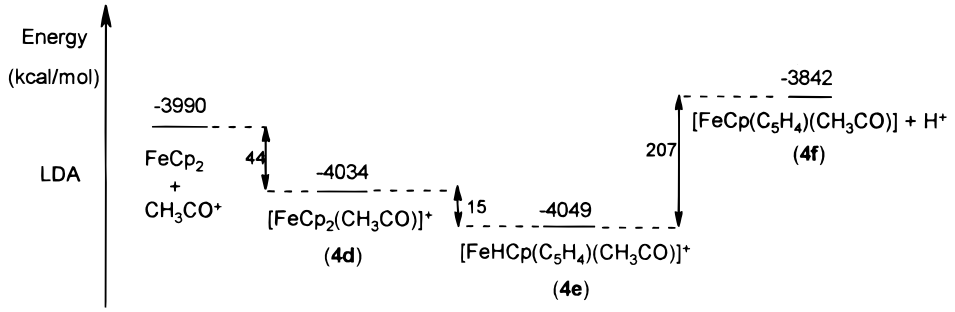

Figure 5. Critical points on the potential energy surface of acetylated ferrocene.

by the acetyl group does not alter the geometry of the ring, and the substituted ring remains more aromatic than the unsubstituted one, where the C−C bonds vary between 1.412 and 1.440 Å. In **4e** the hydrogen facing the proton in the unsubstituted ring is also bent outward from it. Substitution of the Cp ring by a polar system such as an acetyl group does not, thus, substantially affect the structure of the metal-protonated ferrocene. The geometry and energy obtained for **4e** indicates that the acetylation reaction starts with the formation of **4d** to evolve toward the **4e** intermediate with an energy lowering of about 15 kcal/mol. The formation of the **4e** intermediate seems to be the driving force of this electrophilic substitution reaction and stands for an exo mechanism.

To obtain the final product of the exo electrophilic reaction (**4** in Figure 1), a proton should be dissociated from **4e**. It has been suggested that prior to deprotonation a transfer of the proton bonded to the metal may occur to either ring.[20]

The final product of the reaction after the loss of a proton (**4f**) was then optimized. The cis conformation of the acetyl substituent is preferred to the trans one by 0.9 kcal/mol at the LDA level. At this stage, the configuration where the acetyl backbone lies in the same plane as the ring is found to be that of lowest energy. In this conformation the bending angle is almost linear (179.2°) and the unsubstituted ring again planar and aromatic. The C−C bond connecting the acetyl group to the ring is shorter (1.460 Å) than those in structures **4c** (1.658 Å) and **4d** (1.645 Å) (C sp^3 environment) but closer to that of **4e** (1.481 Å) (C sp^2 environment). The metal−ligand distances are also shorter than in the other cases, and they are close to the LDA value in $FeCp_2$. The presence of the electron-withdrawing acetyl group in **4f** enhances the metal to substituted ligand electron donation and shortens the corresponding bond length. Therefore, the metal to unsubstituted ligand donation will be smaller than in $FeCp_2$ and its bond length slightly longer. The critical points on the potential energy surface of acetylated ferrocene are shown in Figure 5.

In attempts to optimize the **4d**, **4e**, and **4f** structures at the B-PW91 level, stable structures were obtained for **4e** and **4f**, whereas geometry optimization of **4d** with the same convergence criteria evolved toward **4e**. Using larger criteria (10^{-3} hartree for the energy and 10^{-2} hartree/Å for the gradients) the structure of **4d** could be optimized. **4e** is now only 3 kcal/mol more stable than **4d**. This energy difference is much lower than that calculated at the LDA level (15 kcal/mol; see Figure 5), indicating the shallowness of the B-PW91 potential energy surface. In **4d**, the metal to substituted and unsubstituted ring distances are longer (1.675 and 1.691 Å, respectively) than those obtained at the LDA level. The $C_{ring}-C_{acetyl}$ bond and the X−Fe−X′ bending angle are now 1.550 Å and 169.8°, respectively. The metal−ligand distances in **4e** are also longer than those

Table 5. Structural Features of Metal-Mercurated Ferrocene (6a) $[FeHgCp_2]^{2+}$, Transition State (6b), and Ring-Mercurated (6c) $[FeCp(C_5H_4)Hg]^+$ Ferrocene at the LDA and B-PW91 Levels of Theory

	6a		6b		6c	
	LDA	B-PW91	LDA	B-PW91	LDA	B-PW91
			Distances *d* (Å)			
Fe−X[a]	1.700	1.762	1.610/1.700	1.660/1.695	1.590/1.632[b]	1.646/1.690
Fe−Hg	2.637	2.721	3.660	3.821	3.870	3.996
Fe−C	2.039−2.165	2.091−2.227	1.967−2.165	2.009−2.170	1.891−2.052	1.928−2.111
C−C	1.412−1.432	1.422−1.443	1.412−1.432[c]	1.422−1.443[c]	1.422−1.430	1.431−1.443
C−H	1.091−1.098	1.085−1.091	1.091−1.098[c]	1.085−1.091[c]	1.090−1.092	1.085
C−Hg	2.762	2.870	2.246	2.335	2.271	2.339
			Angles α (deg)			
X−Fe−X′ [a]	154.4	154.6	169.5	169.0	172.0	172.0
X−Fe−Hg	102.8	102.7	68.5	67.0	62.5	61.0
			Angles *θ* (deg)			
H−C−C′−H′ [a]	0.0	0.0	0.0	0.0	−2.9	0.0
H−C−Fe−Hg	0.0	0.0	0.0	0.0	−1.8	−0.1
			Energy[d]			
	−4.748 913	−4.317 768	−4.949 758	−4.520 642	−4.969 946	−4.539 297
	−2979.99	−2709.06	−3106.02	−2836.75	−3118.69	−2848.45

[a] X and X′ are dummy atoms located in the center of each Cp ring. Similarly, C−H and C′−H′ refer to bonds belonging to different Cp rings. [b] The first value is the metal to upper or substituted ring distance; the second value is that corresponding to the lower or unsubstituted one. [c] These values have not been optimized during the TS search. [d] Energy relative to the spherically averaged ground-state atomic fragments. The first value is given in au and the second in kcal/mol.

obtained at the LDA level (1.679 and 1.682 Å to the substituted and unsubstituted rings, respectively), the bending angle is 1.5° larger, the Fe−H bond is shorter (1.624 vs 1.668 Å), and the H atom is closer to the unsubstituted ring and is at a longer distance from O of acetyl (1.364 and 1.578 Å for $H-C_{unsubstituted-ring}$ and 2.025 and 1.544 Å for $H-O_{acetyl}$, at the B-PW91 and LDA levels, respectively) than at the LDA level. The **4e** structure suggests that the transfer of H preferably proceeds through the unsubstituted ring.[42] Finally, the product of the electrophilic substitution reaction **4f** was also obtained. An elongation of the metal−ligand distances is also observed (1.659 and 1.669 Å to the substituted and unsubstituted rings, respectively). The C−C bond between the ring and the acetyl group is longer as well (1.481 Å), and the system is again practically linear (178.5°).

2.3. Mercuration of Ferrocene. In contrast to protonation and acetylation, mercuration of ferrocene is an example of an electrophilic substitution reaction by a soft electrophile. Experimentally,[21] the reaction has been found to follow an endo mechanism (pathway (b) of Figure 1).

However, as mercuration of ferrocene may conceivably occur via an exo or an endo attack, the two possibilities have again been investigated at the LDA and B-PW91 levels of theory. Actually, the exo mechanism is not very likely since, according to experiment,[21] the acidity of the ring-mercurated metal-protonated system (**2** in Figure 1) would immediately lead to hydrolysis of the C−Hg bond, thus preventing the evolution of the reaction toward the final product of the exo electrophilic substitution.

On the basis of our calculations, no stable structure was obtained for the exo reaction path. With regard to the endo mechanism, the structure of metal-mercurated ferrocene **6a** (Figure 6) was optimized. The results assuming global C_{2v} symmetry are displayed in Table 5. The bending angle is smaller than in the analogous metal-protonated ferrocene. The metal−ligand and metal−electrophile distances are also longer than in the metal-protonated system, due to the larger size of Hg^{2+}. However, the geometry of the ligands is not affected by this larger electrophile and it remains practically the same as in the metal-protonated system.

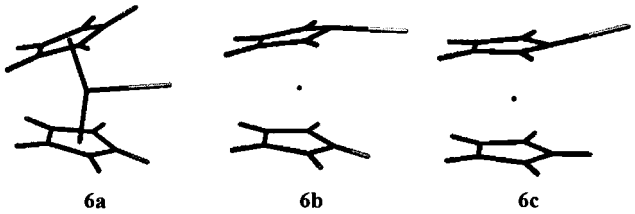

Figure 6. LDA structures for mercurated species.

The structure of the final product (**6c** in Figure 6) was also optimized, and the results are shown in Table 5. The molecule is slightly bent, with a bending angle of 172° at both the LDA and B-PW91 levels of theory. The metal−ligand distances become shorter than those of the **6a** metal-mercurated system. The ligands keep their aromacity and planarity, the C−C bond lengths varying between 1.422 and 1.430 Å at the LDA level and 1.431−1.443 Å at the B-PW91 level. The electrophile is 8.8 and 11.0° out of the plane of the Cp ring it is bonded to, at the LDA and B-PW91 levels of theory, respectively, and points away from the metal atom.

According to an endo mechanism, metal-mercurated ferrocene should evolve toward a structure with the electrophile bonded to the endo face of one of the Cp ligands (structure **6** in Figure 1). Then, the exo proton would be removed so as to obtain the final product of the mercuration reaction. The transition state (TS) for this reaction was searched by an accurate linear transit scan due to the difficulties encountered with the standard transition state optimizing procedure. The distance of the exo proton was elongated step by step up to a reasonable limit of chemical bonding (2.63 Å).

(42) The experiments[20] which were carried out with deuterated ferrocene derivatives indicate that the mode of deprotonation is determined through the retention of C−D bonds. In the case of undeuterated ferrocene it appears that deprotonation through the unsubstituted ring is favored.

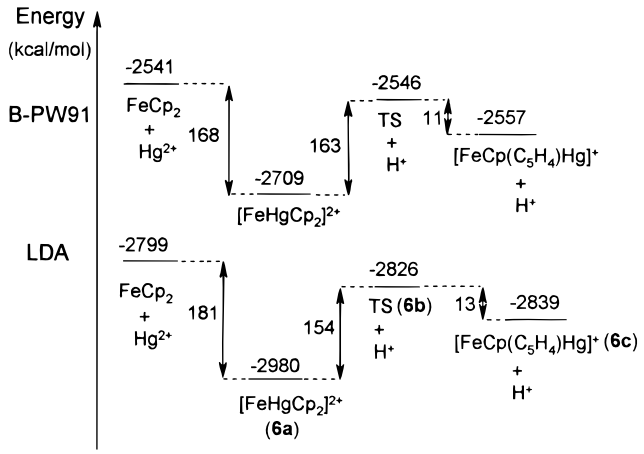

Figure 7. Critical points on the potential energy surface of mercurated ferrocene.

Removing the exo proton from the latter structure and adding the ADF energy of the isolated H^+ to the remaining $[FeCpC_5H_4Hg]^+$ system, the energy still increases by about 40 kcal/mol, now being higher than that of the product (**6c**) plus the isolated H^+. This indicates that the TS might correspond to a system without the exo proton. We have therefore performed some single-point LDA calculations for geometries intermediate between the latter $[FeCpC_5H_4Hg]^+$ structure and the product **6c** to locate the TS. This has led us to a TS (**6b** in Figure 6), i.e., to a structure characterized by a single imaginary vibrational frequency. The energy difference between this LDA transition state (plus the isolated proton) and **6a** is 154 kcal/mol, whereas it is 13 kcal/mol between **6b** and **6c**. The respective values at the B-PW91 level are about 163 and 11 kcal/mol. The structural features for the TS at both levels of theory are reported in Table 5. Figure 7 shows the critical points on the potential energy surface of mercurated ferrocene.

Conclusions

The DFT method at the B-PW91 level of calculation with a triple-ζ STO basis set and a full optimization of the structures has been found to lead for ferrocene to structural and energetic results in excellent agreement with experiment. Thus, this level of theory was expected to yield reliable results also in the case of the mechanism of electrophilic substitution reactions of ferrocene. To this end, typical electrophiles have been selected: proton and acetyl cation as representative of hard systems and Hg(II) as a model of soft ones. In particular, the mechanism of exo versus endo attack has been investigated for these three systems. The important points resulting from this theoretical study, which are in good agreement with a previous study of the chemical reactivity of ferrocene using thermal extensions of DFT,[43] are as follows.

(1) In the case of protonation, no evidence is found for direct exo attack. However, two minima lying at very close energies are predicted on the potential energy surface, the first one corresponding to a metal-protonated system and the second one to an agostic proton located between the metal and the ring. The calculations reveal an extremely shallow potential energy surface between these two minima. Vibrational analysis for a full characterization of the stationary points proved to be necessary. Actually, our results stand for a very rapid equilibrium between metal-protonated and agostic ring-protonated ferrocene. The calculated proton affinities also are in excellent agreement with experiment. These results are at variance with a previous ab initio study by McKee that finds a large energy difference between metal- and ring-protonated ferrocene.

(2) For acetylation exo attack is clearly favored, in agreement with experimental evidence formulated for hard electrophiles. The calculations show that a stable structure is first obtained with a substituted ring carrying the acetyl on the exo face. Then, as the reaction goes on, a metal-protonated intermediate is found leading to acetylated ferrocene as the reaction product. These results suggest that the formation of this intermediate, which has not been trapped in experiments, is the driving force of this reaction.

(3) Finally, as expected for soft electrophiles, mercuration occurs via endo attack. The structures obtained in this case agree with a first precomplexation of the metal and evolution toward mercurated ferrocene through bonding of the electrophile to the endo face of one of the Cp ligands and loss of the proton in an exo position.

The present results show that DFT calculations performed at the B-PW91 level are adequate to discuss and predict the reactivity of metallocenes toward electrophiles.

Acknowledgment. This work is a part of Project 20-49037.96 of the Swiss National Science Foundation. We are grateful to the Centro Svizzero di Calcolo Scientifico in Manno, Switzerland, for a generous grant of computer time.

OM980218I

(43) Grigorov, M. G.; Weber, J.; Vulliermet, N.; Chermette, H.; Tronchet, J. M. J. *J. Chem. Phys.* **1998**, *108*, 8790.